PCCP

Imaging Studies of Photodegradation and Self-healing in Anthraquinone Derivative Dye-doped PMMA

Journal:	*Physical Chemistry Chemical Physics*
Manuscript ID	CP-ART-10-2020-005426.R1
Article Type:	Paper
Date Submitted by the Author:	23-Nov-2020
Complete List of Authors:	Anderson, Benjamin; Washington State University, Applied Sciences Labratory Kuzyk, Mark; Kuzyk, Physics

PCCP

ARTICLE TYPE

Cite this: DOI: 00.0000/xxxxxxxxxx

Imaging Studies of Photodegradation and Self-healing in Anthraquinone Derivative Dye-doped PMMA

Benjamin R. Anderson,*[a] and Mark G. Kuzyk,[b‡]

Received Date
Accepted Date

DOI: 00.0000/xxxxxxxxxx

We study photodegradation and self-healing of nine different anthraquinone-derivatives doped into PMMA using transmission imaging microscopy in search of structure-property relationships of the underlying mechanisms. We find that seven of the nine anthraquinone derivatives display partially reversible photodegradation, with 1,8-Dihydroxyanthraquinone (Dantron/Chrysazin) having the best photostability and recovery characteristics of all dyes tested in this study. Based on these measurements we predict that a sample of 1,8-Dihydroxyanthraquinone doped into PMMA with a concentration of 9 g/l will have a record setting irreversible inverse quantum efficiency of $B_\varepsilon = 4.56 \times 10^9$. Additionally, by considering the performance of the different anthraquinone derivatives and their structures, we develop three rules-of-thumb to qualitatively predict the photostability and recovery characteristics of anthraquinone derivatives. These rules-of-thumb will help guide future experiments and molecular modeling in discerning the underlying mechanisms of reversible photodegradation. Finally, we compare our results for disperse orange 11 dye-doped PMMA to the extended Correlated Chromophore Domain Model (eCCDM). While the eCCDM correctly predicts the behavior of the reversible decay component, it fails to correctly predict the behavior of the irreversible degradation component. This implies further modifications to the eCCDM are required.

1 Introduction

In general, photodegradation of organic dyes is an irreversible process that fundamentally limits their usefulness in optical devices. For several decades much research has been performed to understand organic dyes' photodegradation and determine ways to mitigate its effects[1–13]. Despite these efforts producing major improvements in photostability, all of these improved dyes eventually become unusable due to irreversible photodegradation. However, in 1998 a new phenomenon – self-healing (i.e., reversible photodegradation) – was observed by Peng and coworkers in Rhodamine B and Pyrromethene dye-doped (poly)methylmethacrylate (PMMA), in which degradation of fluorescence was found to be followed by a small degree of recovery[14].

In Peng et al.'s work the observation of self-healing was a minor component that wasn't explored further. However, the phenomenon of self-healing resurfaced several years later with the observation of reversible photodegradation in disperse orange 11 (DO11) dye-doped PMMA using amplified spontaneous emission (ASE),[15] which then opened a wide field of study on reversible photodegradation in dye-doped polymers, with the following materials found to display reversible photodegradation: disperse orange 11 (DO11) dye-doped PMMA,[15–29] DO11-doped PMMA with dispersed ZrO_2 nanoparticles,[30] DO11-doped polyactic acid,[31], DO11-doped polystyrene,[28] DO11 dye-doped copolymer of styrene and MMA,[32] anthraquinone-derivative-doped PMMA,[33–35] 8-hydroxyquinoline (Alq) dye-doped PMMA,[36] air force 455 (AF455) dye-doped PMMA,[37,38] and Rhodamine 6G-doped polyurethane with dispersed Zirconia and Yttria nanoparticles.[39–41]

While the number of materials displaying reversible photodegradation has expanded since 2002, the testbed material in this field continues to be DO11-doped polymers. This continued focus on DO11 has led to the development of the extended Correlated Chromophore Domain Model (eCCDM),[18–20,24–26,28] which describes reversible photodegradation and recovery in DO11/PMMA. This model posits that DO11 molecules aggregate to form domains within the PMMA matrix, with these domains facilitating self-healing through molecular interactions. The mechanism of domain formation is still an open question, with the leading hypothesis being that DO11 molecules hydrogen bind to the same PMMA chain form a domain[19,42].

For completeness we also note that there is a competing hypothesis for DO11/PMMA called the photothermally induced chemical reactions (PTCR) hypothesis.[34] In this hypothesis absorbed light heats both the polymer and dye causing thermal degradation and the formation of radicals and free monomers. Through photocycloaddition, a monomer and a DO11 molecule

[a]Applied Sciences Laboratory, Institute for Shock Physics, Washington State University, Spokane, WA 99210-1495 E-mail: braderson@wsu.edu
[b]Physics Department, Washington State University, Pullman, WA 99164

form a metastable molecule (DO11-MMA oxetane), which eventually decomposes back into pure DO11. The PTCR hypothesis proposes that this metastable molecule is the reversibly damaged species.

If this hypothesis is true, then making minor modifications to the chemical structure of the dye would drastically impact the photodegradation and self-healing properties. Fortunately this can be easily tested for DO11, as it belongs to a class of dyes called anthraquinones that consist of a vast number of variations. These variations include different groups attached to a central molecule at eight different sites, which allows for testing both changes in chemical formula as well as different symmetries for the same chemical formula. A measure of the decay and recovery characteristics of different anthraquinone derivatives will determine how the chemical structure impacts these characteristics and provide insights into domain formation.

Based on this motivation we perform imaging studies of photodegradation and self-healing in nine different anthraquinone derivatives doped into PMMA with a dye concentration of 3 g/l. Based on these measurements we compare the photodegrdation rates and recovery properties of each dye and correlate their values to their molecular structure. These correlations lead us to formulating three rules-of-thumb to qualitatively describe reversible photodegradation in anthraquinone derivative doped PMMA. Additionally we test the concentration dependence of the eCCDM using DO11 and find that the *irreversibly damaged species* does not behave as predicted by the current eCCDM, which implies further development work is required to improve the eCCDM.

2 Background

2.1 Comparison To Other “Self-healing" Materials

To place our work in context requires that we define what we mean by self healing. There are two commonly used definitions in the context of organic chromophores and polymers that are distinct from our work. They are self-healing polymers and reversible “photobleaching”. Self-healing polymers are designed to repair themselves after damage (typically mechanical failure) by the inclusion of repair chemicals inside of the polymer matrix. These polymers, in turn, fall into two separate classifications[43,44]: autonomic (i.e., fully self-contained)[45] and non-autonomic (i.e., requires external stimuli to heal)[46–52]. In autonomic polymers, damage to the polymer results in the release of embedded chemicals (e.g., monomer and catalysts stored in micro-capsules) that subsequently repair the damage; while non-autonomic polymers contain repair chemicals that can be activated via an external stimulus (e.g., heat or light).

Reversible “photobleaching” is the reversible transition of a chromophore from a light emitting state into a dark state (i.e., a form that doesn’t fluoresce). Thus far, the only chromophores found to display this behavior are fluorescent proteins,[53–55] which reversibly “photobleach" through cis-trans photoisomerization.[54] While the literature calls this process “photobleaching," it does not fit the canonical use of the term, which usually refers to processes by which a chromophore dissociates (and/or bond cleavage), which leads to chemical reactions with surrounding molecules. The underlying mechanism of reversible “photobleaching” – photoinduced isomerization – represents a reversible change in configuration of a molecule and not the formation/breaking of new chemical bonds. Therefore it would seem inappropriate to use the term “photobleaching" to describe this process.

The phenomenon of self-healing dye-doped polymers differs significantly from both self-healing polymers and reversible “photobleaching" in that an intrinsic property of the material changes(i.e., no additional chemicals are added) and represents the reversal of *true* photobleaching, with the dyes found to undergo bond cleavage/dissocation followed by the reverse process through chemical reactions.[20,34] In this phenomenon, self-healing is typically used to describe changes to dye molecules, with the polymers acting as the mediating host. There is evidence that this relationship is mutually beneficial, where polymer damage is also found to be repaired in the presence of molecular dopants.[38] Note that while the polymers used in these studies (e.g., PMMA, Polystyrene, Polyurethane) are transparent in the visible regime, they can still be damaged by thermal effects due to localized heating caused by dye molecules absorbing light.

2.2 Possible Photochemistry

To date, precise photochemical models of reversible photodegradation in different dye-doped polymers does not exist and is an area of active research. Four candidate photochemical mechanisms have been proposed for photodegradation and self-healing in DO11[17,19,34,42,56] and 1-AAQ[34] dye-doped PMMA. These four proposed mechanisms are: photo induced intramolecular proton transfer (IPT) tautomerization,[17] self-healing through twisted intramolecular charge transfer (TICT) formation,[56] formation of domains of dye molecules through hydrogen-bonds with the polymer,[19,42] or reversible photocycloaddition.[34].

Photoinduced IPT tautomerization posits that an absorbed photon results in the transfer of a proton from the amine group to the adjacent carbonyl group, which leaves an N-H bond and forms a new O-H bond.[17] See Figure 2 for reference to DO11’s (dye A) molecular structure. The resulting excited IPT state then radiatively relaxes into a tautomer state, which can either nonradiatively decay to the ground state of DO11, or form dimers with other tautomerized DO11 molecules. These dimers are proposed to quench fluorescence, which makes them candidate molecules for the damaged species seen by fluorescence and ASE measurements. Recovery occurs when the less energetically favorable dimers nonradiatively decay to the energetically favorable single DO11 molecules.

The next proposed mechanism, TICT formation, was proposed by Westfall and Dirk based on Hartree-Fock models of the DO11 molecule.[56] In this scenario a DO11 molecule absorbs an incident photon and the molecule twists out of the molecular plane, which is proposed to be the damaged state. Gas-phase Energy surface calculations suggests that the TICT process is more energetically favorable than IPT, but the molecule was not modeled with solvent interactions included.

While both the IPT and TICT mechanism do not rely on the

polymer host to function, domain formation and reversible photocycloaddition are mechanisms that require the presence of a polymer host. In the domain formation description, DO11 tautomers form hydrogen bonds with PMMA chains.[19,42] If N DO11 molecules bond with a given PMMA chain, that structure is called a domain of size N. These molecules can interact with each other through polymer-mediated phonons or excitons,[20,25] which results in the observed self-healing phenomenon. Under this framework, photodegradation is proposed to result in photodissociation of dye molecules, with the domains trapping fragments, which can subsequently recombine resulting in self-healing.

The final proposed mechanism is photocycloaddition. In general, cycloaddition involves unsaturated molecules combining to form a cyclic adduct. In the case of DO11/PMMA, the reaction is between DO11 and MMA monomers, which are formed by localized photothermal heating of the polymer due to dye molecules absorbing light. It has been proposed that this photothermal reaction between DO11 molecules and MMA monomers forms DO11-MMA oxetane, which is metastable.[34] Once formed this complex has a limited lifetime and eventually decomposes to give a pristine DO11 molecule. This relaxation results in the observation of self-healing.

Note that the first two proposed mechanisms (IPT tautomerization and TICT state formation) are independent of the polymer and would suggest that self-healing can occur in solution. However, self-healing of DO11 and 1-AAQ has not been observed in solution to date. Therefore these proposed mechanisms are not likely to be accurate explanations. However, both the domain model and reversible photocycloaddition rely on the polymer host to to function and are therefore both viable explanations.

2.3 Phenomenological Models

At present three phenomenological models predict experimental observations of reversible photodegradation: a two- or three-populaton non-interacting model and the extended correlated chromophore domain model (eCCDM). In this section we will provide a brief overview of the three models, with further details available in previous publications[21,26,27,57].

2.3.1 Non-interacting Models

2.3.1.1 Two Species Model The first and simplest phenomenological model used in this study is the two-species non-interacting model (NIM). This model is a two species model developed by Embaye and Kuzyk, in which undamaged molecules reversibly transition into a damaged state during photodegradation and then relax back to the undamaged state when left in the dark[17].

During photodegradation ($t \leq t_D$) the damaged population's fractional number density is given by[17]:

$$n(t) = 1 - \frac{\beta}{\beta + \alpha_2 I_p} - \frac{\alpha_2 I_p}{\beta + \alpha_2 I_p} e^{-(\beta+\alpha_2 I_p)t}, \tag{1}$$

and during recovery ($t > t_D$) it is given by

$$n(t) = [1 - n(t_d)]e^{-\beta(t-t_D)}, \tag{2}$$

where t_D is the time at which the pump is turned off, α_2 is the decay rate parameter, I is the pump intensity, and β is the recovery rate. This model was developed based on measurements using ASE in DO11/PMMA that displayed full recovery after degradation. However, it was later revealed – using imaging – that the sensitivity of ASE and imaging to the irreversibly damaged product are different, thus leading to a different measure of recovery.[21]

This irreversible damage can be accounted for in the two population model by revising the population functions to be

$$n(t) = \begin{cases} [n_2(I_p,t_D) + n_1(I_p,t_D)](1 - e^{-(\beta+\alpha_2 I_p)t}) & t \leq t_D \\ n_2(I_p,t_D) + n_1(I_p,t_D)e^{-\beta(t-t_D)}, & t > t_D \end{cases} \tag{3}$$

where $n_1(I,t_D)$ is recoverable portion and $n_2(I,t_D)$ is the irreversibly damaged portion. While Equation 3 describes the damaged population's dynamics, in practice transmission imaging microscopy does not directly measure the populations, but instead measures the intensity of light transmitted through the sample at a given time and position (x,y) $C(x,y,t)$ as measured with a CCD array. This intensity can be converted to a scaled damaged population (SDP) using,[21,35]

$$n'(x,y,t) = -\ln\left(\frac{C(x,y,t)}{C_0}\right) \tag{4}$$

$$= \Delta\bar{A}(x,y,t), \tag{5}$$

where C_0 is the background pixel intensity and $\Delta\bar{A}(x,y,t)$ is the frequency averaged change in absorbance at point x,y and time t.

The SDP can be expressed in terms of the two damaged populations as,

$$\Delta\bar{A}(x,y,t) = \Delta\bar{\sigma}_1 L n_1(x,y,t) + \Delta\bar{\sigma}_2 L n_2(x,y) \tag{6}$$

where we have used the thin sample approximation (i.e., the sample is so thin as to have negligible pump depletion), L is the sample thickness, and $\Delta\bar{\sigma}_i$ is the frequency averaged cross section for the i^{th} population. The frequency averages over the LED spectrum which results in the camera measuring a range of wavelengths. This broad spectrum results in the camera's intensity values being a convolution over spectral components given by

$$\Delta\bar{\sigma}_i = \int_0^\infty d\omega f(\omega)\Delta\sigma_i(\omega), \tag{7}$$

where $f(\omega)$ is the combined spectral response of the camera and the probe spectrum and $\Delta\sigma_i(\omega) = \sigma_i(\omega) - \sigma_0(\omega)$ is the frequency dependent difference in cross section, where $\sigma_i(\omega)$ is the population's cross section with $i = 0$ being the undamaged population, $i = 1$ being the reversibly damaged population, and $i = 2$ being the irreversibly damaged population.

2.3.1.2 Three Species Model In the previous section we considered a simple "two"-species model of reversible photodegradation. This model ignored effects due to pump depletion (e.g., pump intensity varying with depth) and addressed the irreversible species in an *ad hoc* fashion. To correctly account for these effects we use a more complex model that is described in

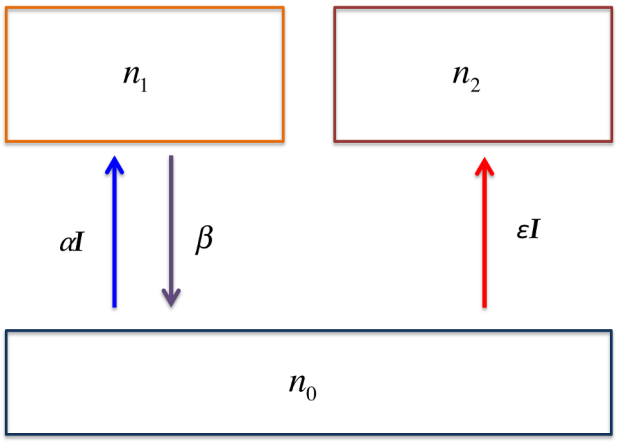

Fig. 1 Diagram showing the three-species population model. Note that the pump intensity depends on depth and time.

detail in Ref's[25–27].

In this model undamaged dye molecules (of fractional number density n_0) decay either reversibly to species #1 (of fractional number density $n_1(z,t)$ at depth z and time t) or irreversibly to species #2 (of fractional number density $n_2(z,t)$ at depth z and time t), with pump depletion accounted for using the Beer-lambert law. Note that for brevity we do not explicitly show the x and y dependence, but this dependence is implied. A simple diagram of species transitions are shown in Figure 1.

In this model the population dynamics and intensity depletion are described using four coupled differential equations[27]:

$$\frac{\partial n_0(z,t)}{\partial t} = -(\alpha+\varepsilon)I_p(z,t)n_0(z,t)+\beta n_1(z,t), \tag{8}$$

$$\frac{\partial n_1(z,t)}{\partial t} = \alpha I_p(z,t)n_0(z,t)-\beta n_1(z,t), \tag{9}$$

$$\frac{\partial n_2(z,t)}{\partial t} = \varepsilon I_p(z,t)n_0(z,t), \tag{10}$$

$$\frac{\partial I_p(z,t)}{\partial z} = -[\sigma_0(\omega_p)n_0(z,t)+\sigma_1(\omega_p)n_1(z,t) + \sigma_2(\omega_p)n_2(z,t)]I_p(z,t). \tag{11}$$

where α is the reversible decay rate parameter, ε is the irreversible decay rate parameter, $I_p(z,t)$ is the depth-dependent pump intensity, and σ_i is the species absorbance per unit length. Note that we can rewrite Equation 11 without dependence on $n_0(z,t)$ by rewriting it in terms of the absorbance difference $\Delta\sigma_i$, which yields,

$$\frac{\partial I_p(z,t)}{\partial z} = -[\sigma_0(\omega_p)+\Delta\sigma_1 n_1(z,t)+\Delta\sigma_2 n_2(z,t)]I_p(z,t). \tag{12}$$

where $\Delta\sigma_i = \sigma_i(\omega_p)-\sigma_0(\omega_p)$.

Using Equations 8-10 we can model the populations as a function of depth and time during photodegradation and recovery. However, as mentioned above, in practice what we measure using transmission imaging is the scaled damaged population ($\Delta\bar{A}(t;\omega)$). Therefore we need to revise Equation 6 to include the effect of depth on the measured SDP and obtain

$$\Delta\bar{A}(t;\omega) = \Delta\bar{\sigma}_1\int_0^L n_1(z,t)dz+\Delta\bar{\sigma}_2\int_0^L n_2(z,t)dz. \tag{13}$$

2.3.1.3 Photodegradation Quantum Efficiency In the above sections we use three parameters (α_2, α, and ε) to characterize the degradation rate(s) for a given pump intensity. While these quantities are directly found when performing experimental fits, they are not overly useful in comparing materials photostability as they depend on the dye's concentration ρ, undamaged molecular absorbance cross section $\varepsilon_0(\omega_p)$, and the pump photon energy $\hbar\omega_p$. Therefore, for our comparisons we will convert the fit parameters to the more useful inverse quantum efficiencies (IQEs) of photodegradation B_i, which are related to the three model parameters by:

$$B_2 = \frac{\rho_M\varepsilon_0(\omega_p)}{\alpha_2\hbar\omega_p}, \tag{14}$$

$$B_\alpha = \frac{\rho_M\varepsilon_0(\omega_p)}{\alpha\hbar\omega_p}, \tag{15}$$

$$B_\varepsilon = \frac{\rho_M\varepsilon_0(\omega_p)}{\varepsilon\hbar\omega_p}. \tag{16}$$

where ρ_M is the number density and $\varepsilon_0(\omega_p)$ is the molar absorbance cross section at the pump frequency ω_p. These inverse quantum efficiencies are commonly used to compare photostability of materials and physically represent the number of photons needed to be absorbed in order to photodegrade a molecule[7]. Therefore the larger a molecule's IQE is, the more photostable it is.

2.3.2 Modeling with Interactions: The Correlated Chromophore Domain Model

The correlated chromophore domain model (CCDM) is a kinetic model of reversible photodegradation that was first developed by Ramini and Kuzyk in 2012 to describe temperature- and concentration-dependent ASE measurements of reversible photodegradation in DO11/PMMA[18,19]. Shortly thereafter the model was extended to describe linear measurements (e.g., imaging) and the effects of an applied electric field[20,25,26]. This extended model has proven to be robust at describing reversible photodegradation in DO11/PMMA for a wide range of experimental conditions.

The fundamental hypothesis of this model is that when dye molecules are doped into PMMA they form linear aggregates that interact in such a way as to improve photostability and give rise to the phenomenon of self-healing. The molecules in these domains have modified decay and recovery parameters that depend on the size of the domain N with the three-species model parameters being modified as follows:

$$\alpha \to \frac{\alpha_1}{N}, \tag{17}$$

$$\beta \to N\beta_1, \tag{18}$$

$$\varepsilon \to N\varepsilon_1, \tag{19}$$

where N is the number of molecules in a domain and α_1, β_1, and ε_1 are the single-molecule values. Hence, the degradation rate α decreases as N increases and the recovery rate β and irreversible decay rate ε increases.

These domains are size-distributed according to a statistical mechanical model with a distribution derived form the grand partition function yielding [18–20]:

$$\Omega(N) = \frac{1}{z}\left[\frac{(1+2\rho z) - \sqrt{1+4\rho z}}{2\rho z}\right]^N, \tag{20}$$

where ρ is a dimensionless density parameter and z is given by

$$z = \exp\left\{\frac{\lambda}{kT} - \eta E_0^2\right\}, \tag{21}$$

with λ being the zero-field free energy advantage (i.e., the binding energy of adding a molecule to a domain), T is the temperature, k is Boltzmann's constant, E_0 is the applied electric field, and η is a parameter proportional to the polarizability of the dye molecules [20].

Based on the distribution of domains (Equation 20) and the decay/recovery parameter dependencies on the domain size we can make predictions on how concentration will influence these parameters. To do so we note that the average domain size is related to the density as $\langle N\rangle \sim \sqrt{\rho z}$. Therefore, when comparing the parameters previously measured for 9 g/l doping [28] to those now measured at 3 g/l doping, we anticipate for both ε and β the 9 g/l samples will have values 1.73 times larger, while α will be 0.577 times smaller.

3 Method

3.1 Sample Preparation

For this study we chose nine different anthraquinone derivatives, whose chemical/trade names and relevant properties are listed in Table 1 and whose structures are shown in Figure 2. To simplify our discussion below we assign each anthraquinone a letter code. For sample preparation we first dissolve the dye into filtered MMA (such that the final dye concentration will be 3 g/l) and sonicate the solution for 0.5 h to insure that the dye is fully in solution. After this initial sonication we add an initiator (butanethiol) and a chain transfer agent (Tert-butyl peroxide) in amounts of 33 μl per 10 ml of MMA, followed by further sonication for 1 h. Once mixed the solution is filtered through a 0.2 μm disk filter into vials that are placed in a 95 °C oven to initiate polymerization. Typically full polymerization is completed within 48 h. The solid dye-doped polymer is then separated from the glass vial by placing it in a freezer, which results in separation due to differential expansion.

From this bulk dye-doped PMMA sample we remove a small portion and placed it between two glass slides to form a sandwich structure. This sandwich is then pressed in a custom oven/press with the temperature maintained at 150°C, which is well above the glass transition temperature of all samples. The uniaxial stress is then gradually increased perpendicular to the sample until reaching 621 kPa at which point the stress is held constant for 1 h. Subsequently, the stress is released and the sample is left to cool.

3.2 Transmission Imaging Microscopy

Transmittance imaging microscope (TIM) probes photodegradation and recovery. [21,27,35] The collimated blue light from a LED is focused on the sample with a microscope objective and the transmitted light imaged with a CMOS camera. The light from a CW Ar:Kr ion laser at either 514 nm or 488 nm is focused onto the sample with a cylindrical lens forming a strip of damage. The power incident on the sample is varied using a half-waveplate/polarizer pair.

The on-sample burn profiles are matched to the incident intensity profile by first measuring the beam profile using the TIM with no sample and neutral density filters placed in front of the camera to protect it. These beam images map the spatial profile of the incident beam. Subsequently, the sample is photodegraded over a time that depends on sample composition. The shortest burn dose is 6 mins, while the longest is 25 min. Recovery is monitored with imaging after degradation at a semi-log sampling rate. Figure 3 shows typical blue channel images taken of DO11/PMMA before degradation, immediately after degradation, and after 24 h of recovery. Figure 3 shows that photodegradation results in an increase in transmittance (i.e., the bright spot), with recovery resulting in the transmission decreasing (i.e., the dim spot).

The images are used to determine the SDP at fifty different locations in the damaged area for each image using Equation 4, which produces a data set of fifty different decay and recovery curves for a wide range of intensities. These curves are then simultaneously fit to either the two-species or three-species NIM with only the intensity and thickness allowed to change from curve-to-curve. Note that the thickness varies as the samples are not uniform. By performing simultaneous fits of all the curves in a data set, we are able to determine one set of fit parameters over the 50 curves with a high degree of accuracy.

4 Results

4.1 Two-species Non-interacting Model Results

We begin our analysis of the SDPs measured during decay and recovery by considering the fit parameters determined using the Two-species NIM. An example of this fitting is shown in Figure 4, with the data from dye K's decay and recovery fit to the Two-species NIM. From these fits we obtain the the two-species decay parameter α_2, the recovery rate β, and the recovery fraction RF, for each spatial location, with the recovery fraction being computed as

$$RF = \frac{n'_R}{n'_{IR} + n'_R}, \tag{22}$$

Table 1 Anthraquinones and relevant parameters. λ_p is the pump wavelength used and ε_p is the absorbance cross section at the pump wavelength.

Dye Code	**Chemical Name**	**Trade Name**	$\lambda_{\mathbf{p}}(\mathbf{nm})$	**Number Density** $(10^{18}\mathrm{cm}^{-3})$	$\varepsilon_{\mathbf{p}}(10^{-18}\ \mathrm{cm}^2)$ [33]
A	1-Amino-2-methylanthraquinone	Disperse orange 11 (DO11)	488	7.6	16
B	1-Amino-2,4-dibromoanthraquinone	–	488	4.7	28
C	1-Amino-4-Hydroxyanthraquinone	Disperse Red 15 (DR15)	514	7.6	3.7
H	1,4 Diaminoanthraquinone	Disperse Violet 1 (DV1)	514	7.6	38
I	1,5 Diaminoanthraquinone	Disperse Red 11 (DR11)	488	7.6	18
J	1,2 Dihydoxyanthraquinone	Alizarin	488	7.5	17
K	1,8 Dihydoxyanthraquinone	Dantron or Chrysazin	488	7.5	29
L	1,4 Dihydoxyanthraquinone	Quinizarin	488	7.5	9.2
P	1-(Methylamino)anthraquinone	Disperse Red 9 (DR9)	514	7.6	7.7

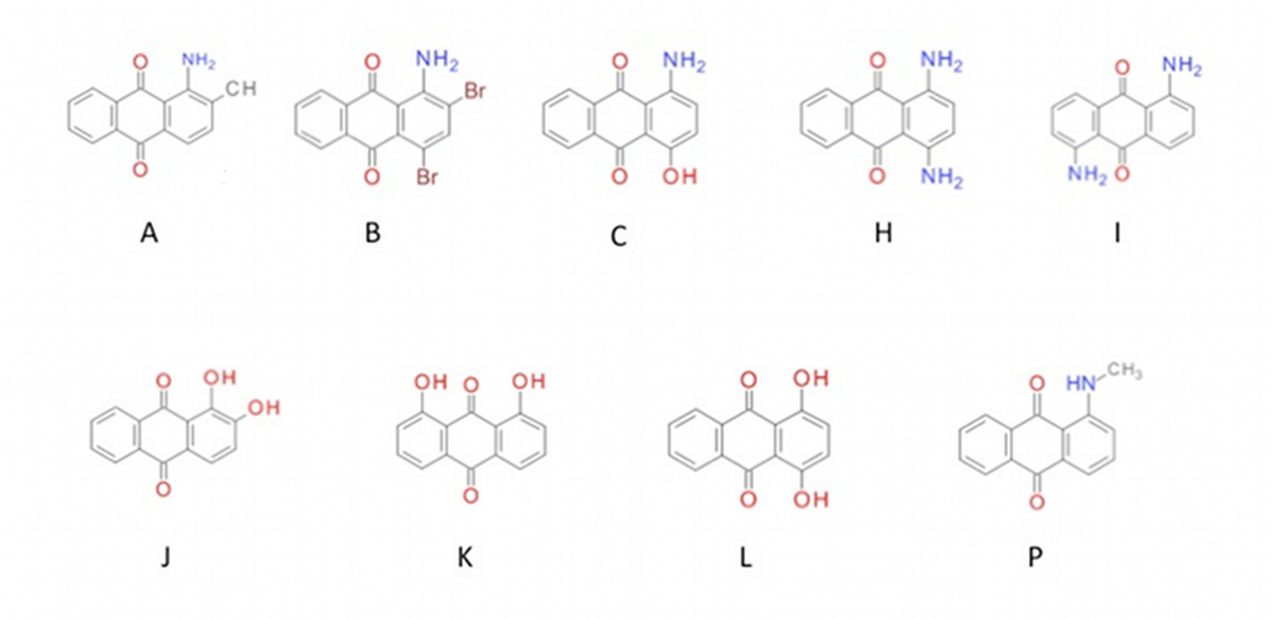

Fig. 2 Schematic structures of the nine anthraquinone derivatives tested in this study.

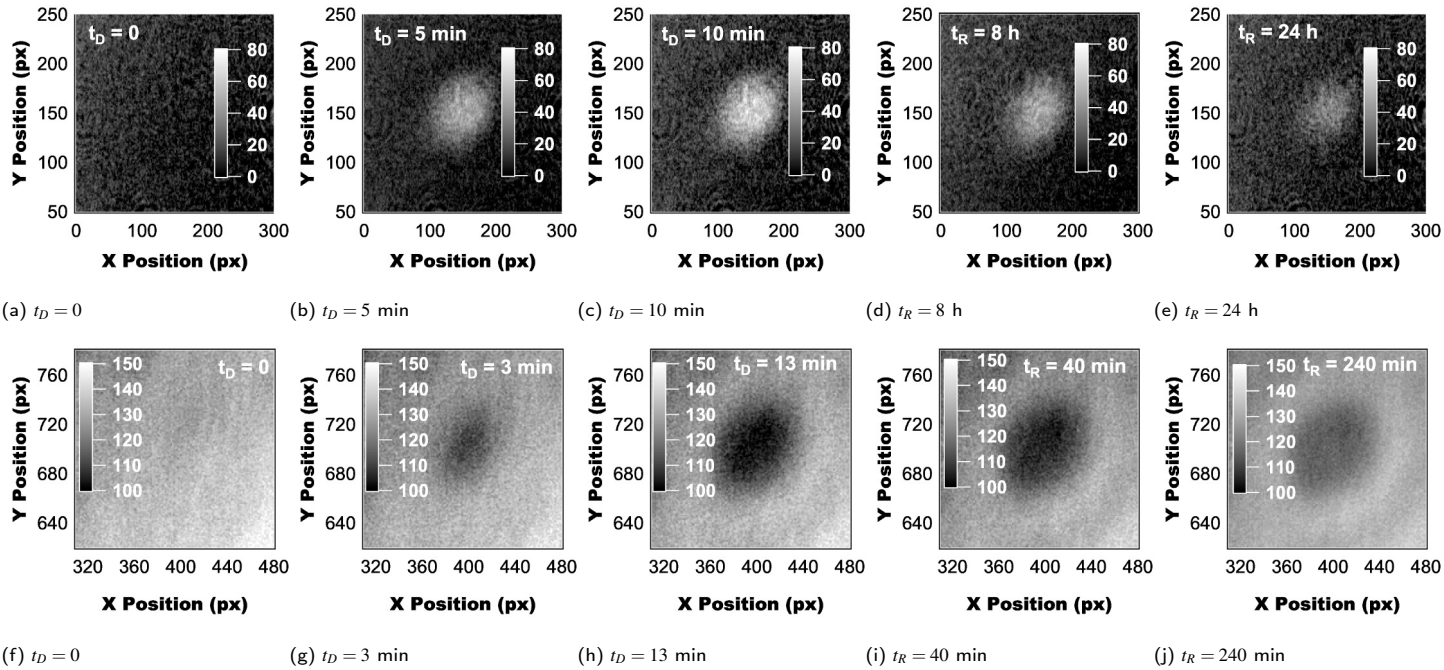

(a) $t_D = 0$ (b) $t_D = 5$ min (c) $t_D = 10$ min (d) $t_R = 8$ h (e) $t_R = 24$ h

(f) $t_D = 0$ (g) $t_D = 3$ min (h) $t_D = 13$ min (i) $t_R = 40$ min (j) $t_R = 240$ min

Fig. 3 Example blue channel images of DO11/PMMA (a-e) and dye K/PMMA (f-j) during photodegradation and recovery. Note that damage in DO11/PMMA results in a decrease in absorption at the probe wavelength (≈ 460 nm) (i.e., brightening of the image), while for dye K damage results in an increase in absorption at the probe wavelength (i.e., darkening of the image). For analysis, fifty different pixels in the damaged area are converted into SDPs using Equation 4.

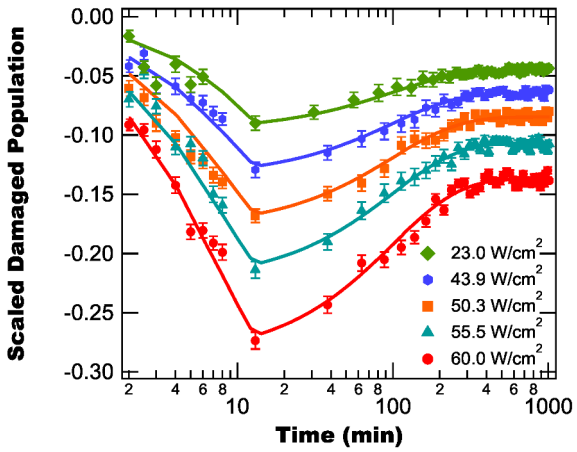

Fig. 4 Example decay and recovery data (points) and fits (curves) as a function of time for different intensities.

where n'_R is the reversible SDP component and n'_{IR} is the irreversibly decayed SDP component. After obtaining these parameters at all fifty locations we compute the average values for α_2 and β as well as the peak recovery fraction, which are listed in Table 2 for all nine anthraquinone derivatives. Once we have obtained an average decay parameter, we then also compute the Inverse Quantum Efficiency for each dye using Equation 14 and the cross sections listed in Table 1.

Table 2 shows that every dye except C and P display measurable recovery, with dye L having the slowest recovery and dye K having the fastest recovery. Based on the maximum recovery fraction observed we find that dye K is once again the best dye, with dye J having slightly less recovery. Dyes A, L and I recover to about 15% and dyes B and H recover less than 10%. Note that (except for dye P) these results are qualitatively consistent with a previous study using fluorescence as a probe technique.[33] In that study weak recovery was observed in fluorescence for dye P, but used significantly lower fluences and a different probe technique. In the discussion section below we will discuss possible mechanisms for the differences in dye performance.

Next we consider the decay parameters listed in Table 2, which are found to range from 0.84×10^{-3} cm^2/(W min) to 9.81×10^{-3} cm^2/(W min), with dye L having the smallest decay parameter and dye A having the largest. While these observations initially suggest that dye L is the most photostable, this is an erroneous conclusion as it neglects the effect of the absorbance cross section (i.e., dye L has relatively low absorbance at the pump wavelength leading to slower decay). When we correct for the influence of absorbance by computing the IQE we find that dye H is the most photostable with an IQE of 2.91×10^6, followed by dye K with an IQE of 1.96×10^6. These values are of the same order of magnitude as many other organic dyes studied for *irreversible* photodegradation[7–13,58].

4.2 Three-species Non-interacting Model

In the above section we considered the two-species NIM parameters for the anthraquinone derivatives and calculated the dye's IQEs, which are comparable to other molecules in the literature[7–13,58]. However, this comparison is deceptive as our two-species analysis lumps both the reversible and irreversible de-

Table 2 Anthraquinone decay and recovery parameters for the two-species model: α_2 is samples two-species decay parameter, β is the recovery rate, and RF is the maximum recovery fraction observed, as this varies across the sample.

Dye	$\alpha_2(10^{-3}\text{cm}^2/(\text{Wmin}))$	$\beta(10^{-3}\text{min}^{-1})$	Rec. Frac	$B_2(10^6)$
A	9.81 ± 0.19	1.65 ± 0.51	0.15	0.2404 ± 0.0047
B	8.21 ± 0.54	2.4 ± 1.4	0.05	0.572 ± 0.043
C	3.60 ± 0.72	0	0	0.150 ± 0.030
H	1.92 ± 0.31	1.58 ± 0.28	0.07	2.91 ± 0.47
I	1.85 ± 0.39	2.04 ± 0.42	0.18	1.43 ± 0.30
J	2.56 ± 0.15	6.5 ± 3.2	0.35	0.980 ± 0.057
K	2.18 ± 0.24	10.0 ± 1.4	0.47	1.96 ± 0.22
L	0.84 ± 0.36	0.91 ± 0.26	0.14	1.61 ± 0.69
P	4.4 ± 1.0	0	0	0.257 ± 0.059

cay parameters into a single value. To correctly compare the anthraquinone derivatives photostability to other molecules we need to separate out the two decay channels and determine their individual IQEs.

Separating the two decay channels requires using the three-species NIM analysis mentioned above (and described in detail in Ref[27]). Therefore we reperform fits of the decay and recovery curves using the three-species NIM and tabulate the results in Table 3. We find that for all dyes except dye B the reversible decay parameter α is larger than the irreversible decay parameter ε, so the reversible decay channel is more likely to occur than irreversible decay. Previously we observed this relationship between α and ε in studies of DO11/PMMA with 9g/l doping, with the proposed hypothesis being that the reversible decay channel is a one step process involving the dye molecule, while the irreversible decay channel involves a two step process requiring absorption by the dye followed by damage to the polymer host[20,23]. This damage is most likely due to thermally induced chain scission and cross-linking[23,59–61] with energy transfer between the dye molecules and the polymer being the source of thermal energy[8,59,62–66]. This hypothesis implies that the irreversible QE, B_ε, is related to the efficiency of this energy transfer.

5 Discussions

5.1 Effect of Concentration on DO11/PMMA Decay and Self-healing

Currently, DO11 (dye A) is the benchmark dye for reversible photodegradation. Numerous studies have been performed on its photodegradation and self-healing resulting in the development of a robust model for its reversible photodegradation (i.e., the eCCDM)[18–20,24–26]. This status as the benchmark dye makes it the ideal starting place for our discussion of the experimental results presented above.

Previously, we performed the same three species analysis described above on a DO11/PMMA sample using a dye concentration of 9g/l[27]. Therefore we can compare the values measured in the previous study to those obtained in this study and determine how closely they match the predictions of the eCCDM. To do so Table 4 tabulates the different parameters from both studies and computes their ratio and compares it to the eCCDM predicted ratio. We find that both α and β behave as expected from the eCCDM (i.e., α increases and β decreases) with the ratio between concentrations being within uncertainty of the value predicted by the eCCDM. This result adds one more piece of evidence that the eCCDM is the correct model of reversible photodegradation for DO11/PMMA.

However, while α and β behave as expected, ε is found to behave counter to the eCCDM prediction, with the lower concentration sample having a faster irreversible decay rate. The eCCDM successfully predicts α and β's concentration dependence, but fails at modeling ε, so further work is needed to better understand how to incorporate the irreversible decay componen into the eCCDM. This wasn't previously observed because the original two-population CCDM[18,19] was tested for its concentration dependence but the eCCDM – which introduced ε – was tested at only one concentration but worked for different temperatures and electric fields.

A full revision of the eCCDM to correctly account for this concentration dependence is beyond the scope of this study and will require testing samples at multiple concentrations. However, we hypothesize that this anomalous concentration dependence may be due to two sources: a concentration dependent ε that is independent of domain size and another one due to the domain size dependence εN. The εN dependence accurately predicts the behavior for different electric fields and temperature but may need to be augmented with a domain-independent contribution.

5.2 Effect of Dye Structure on Reversible Photodegradation

We compare different dye molecules for their photostability and recoverability through their reversible and irreversible IQEs as well as their recovery rates and recovery fractions, which are given in Tables 2 and 3. Based on these four parameters we rank the dyes as follows (from worst to best): Dyes C and P have the worst characteristics of any dye tested with neither dye displaying appreciable recovery. Next is Dye B, which shows recovery, but only a small amount ($< 5\%$) and has the smallest irreversible IQE. The next three dyes are more nuanced with dyes A, L and I having better recovery parameters than dye H, but dye H being more photostable than all three. However, it does not recover as well. After these intermediate dyes, dye J comes in with significant improvement in recovery and a larger irreversible IQE, but a smaller reversible IQE. Thus dye J's preferred decay channel is re-

Table 3 Three-species NIM model decay parameters and their corresponding inverse quantum efficiencies.

Dye	$\alpha(\mathbf{10^{-3}cm^2/(Wmin)})$	$\varepsilon(\mathbf{10^{-3}min^{-1}})$	$\mathbf{B}_\alpha(\mathbf{10^6})$	$\mathbf{B}_\varepsilon(\mathbf{10^6})$
A	7.27 ± 0.44	2.26 ± 0.19	0.324 ± 0.020	1.044 ± 0.086
B	4.9 ± 2.0	6.3 ± 1.9	0.84 ± 0.35	0.652 ± 0.20
H	1.36 ± 0.48	0.88 ± 0.46	4.2 ± 1.5	6.3 ± 2.1
I	2.68 ± 0.16	0.512 ± 0.072	0.989 ± 0.059	5.18 ± 0.73
J	3.24 ± 0.46	0.256 ± 0.071	0.77 ± 0.11	9.8 ± 2.7
K	3.80 ± 0.25	0.124 ± 0.022	1.125 ± 0.073	34.481 ± 2.4
L	0.91 ± 0.16	0.192 ± 0.044	1.50 ± 0.26	7.051 ± 1.6

Table 4 Decay and recovery parameters for DO11/PMMA prepared at concentrations of 9 g/l[27] and 3 g/l (this study) with the ratio between parameters at each concentration and the predicted ratio from the mCCDM.

Parameter	9 g/l	3 g/l	Measured Ratio	Predicted Ratio
$\alpha(\mathbf{10^{-3}cm^2/(Wmin)})$	4.40 ± 0.34	7.27 ± 0.44	0.606 ± 0.059	0.577
$\beta(\mathbf{10^{-3}min^{-1}})$	3.88 ± 0.47	1.65 ± 0.51	2.35 ± 0.76	1.73
$\varepsilon(\mathbf{10^{-5}min^{-1}})$	3.60 ± 0.34	226 ± 19	$1.59(\pm 0.61) \times 10^{-2}$	1.73

versible, albeit with a lower IQE than some of the other dyes. The best dye found in this study is dye K, which has a recovery rate almost an order of magnitude higher than the other dyes, significantly higher recovery fraction, and an outstanding irreversible IQE.

While dye K's irreversible IQE for 3 g/l doping is slightly above the average values seen in the literature,[7–13,58] we find tantalizing evidence that at higher concentrations it may actually have a record setting irreversible IQE. In a previous study of DO11 we measured $B_\varepsilon \approx 1.4 \times 10^8$ for a 9 g/l sample.[27] If the IQE ratio between DO11 and dye K is the same at 9 g/l doping, then dye K would have an irreversible IQE of 4.56×10^9. This value – to the best of our knowledge – is larger than any other IQE published in the literature. This would make dye K-doped PMMA one of the most resilient materials to *irreversible* photodegradation. However, we note that while this prediction is very promising it must be experimentally verified.

With these rankings, we speculate on how the molecular structure correlates with improvement in performance. From Figure 2, we find that dyes with OH groups that straddle the same oxygen (dyes J and K) have the best recovery performance, with the 1,8 position being the best configuration. On the other hand, dye L with OH groups associated with different oxygens does not aid in reversibility, but does help with photostability.

In the case of molecules with a NH_2 group in the 1 position, we find that the majority of these dyes recover, but with a wide range of performance that depends on the other attached groups. As with the OH groups we find that having two NH_2 groups in both the 1 and 4 positions improves photostability, but does not lend to increased recovery, with the most extreme example being the mixed dye C, which has an NH_2 at position 1 and an OH at position 4. Finally, one of the most interesting results for this group of molecules is the drastically different performance of dyes H and I which have the exact same chemical formula, but differ in the symmetry of the NH_2 groups. Dye H is more photostable but with poorer recovery, while dye I is less photostable, but has improved recovery.

Based on these observations (and previous studies on anthraquinone derivatives[33,34]) we provide the following rules of thumb to describe the photostability and recovery characteristics of anthraquinone derivatives:

1. For recovery to be possible there needs to be an OH or NH_2 group in position 1.

2. Groups placed in both the 1 and 4 positions simultaneously result in decreased self-healing properties, but increased photostability.

3. Groups placed on opposite sites of the oxygen axis (e.g., positions 1 and 8) result in improved self-healing.

Further tests of these rules of thumb are needed to confirm their validity with these future studies needing to consider the photodegradation and self-healing properties of 1,8 Diaminoanthraquinone, 1,2 Diaminoanthraquinone, 1,5-Dihydroxyanthraquinone (Anthrarufin), and 1-Amino-5-hydroxyanthraquinone. These four dyes are essentially permutations of the ones already tested and are therefore good tests of these rules of thumb. Based on theses three rules we anticipate that: 1,8 Diaminoanthraquinone and 1,2 Diaminoanthraquinone will have very good recovery, 1,5-Dihydroxyanthraquinone will have decent recovery (but less than dye K), and that 1-Amino-5-hydroxyanthraquinone will both recover better and be more photostable than dye C.

While these rules of thumb can help guide us towards more photostable and better healing anthraquinones, they still do not identify the underlying mechanisms of reversible photodegradation and the physics/chemistry behind its dependence on anthraquinone structure. To utilize these results to better understand the underlying mechanisms we need to turn back to the eCCDM, with the assumption that the eCCDM is the correct model

for all self-healing anthraquinones (which is an assumption to test in a future study).

In the eCCDM the degradation and recovery properties depend on the domain size, which is determined by the free energy advantage λ, temperature, applied electric field, and density. For DO11/PMMA, λ is found to be ≈ 0.3 eV, which is about the same energy as hydrogen bonding between a DO11 dye molecule and the PMMA backbone. This similarity has led to the proposal that domain formation is due to hydrogen bonding between the DO11 dyes and the PMMA backbone.[19,42]* This bonding leads to the dye molecules in a domain being correlated through the polymer chain with interactions being mediated by excitons and/or phonons.[20,25] If this is the actual bonding mechanism, then a computational study of bonding between each anthraquinone derivative and PMMA could reveal how the free energy advantage (i.e., the bonding energy) varies with dye structure. From previous modeling and tests on DO11 in different polymers[20,30] we know that larger free energy advantages result in larger domain sizes, which correlate with improved healing. This could very well explain why 1,8-Dihydroxyanthraquinone has such remarkable properties as it has two OH groups on the same side that can contribute to hydrogen bonding with the polymer.

6 Conclusions

We measure photodegradation and self-healing in anthraquinone derivative-doped PMMA samples for nine different anthraquinones. We determine that seven out of the nine anthraquinone derivatives display self-healing with 1,8-Dihydroxyanthraquinone found to have the best self-healing properties of any dye tested. Based on these measurements and the chemical structures of the anthraquinones we determine three rules-of-thumb for qualitatively predicting the photostability and self-healing capabilities of anthraquinone derivatives and provide candidates for future study to test these rules of thumb. We also propose an explanation for the structure dependent recovery properties, with the underlying mechanism being related to the hydrogen binding energy between the dye and the PMMA backbone.

Additionally, we perform the first test of the eCCDM's concentration dependence and find that while the eCCDM successfully predicts the behavior of the reversible species for different concentrations, it fails to correctly describe the irreversible species concentration dependence. This suggests that further development work is required to correct the eCCDMs concentration dependence, with the most likely candidate being that the single-molecule-domain irreversible decay parameter ε_1 depends on concentration. To better understand this observation a future study will consider the concentration dependence of the irreversible species.

* While this bonding can be probed in theory using FTIR spectroscopy, the one FTIR study on these materials required a concentration of 105 g/l to obtain decent signal.[34] Such a large concentraion is almost certainly not representative of our current samples that have a concentration of 3 g/l.

Acknowledgements

We would like to thank Prabodh Dahkal and Elisao DeLeon for their help preparing samples for this study.

Funding Information

This work was supported by Wright Patterson Air Force Base, Air Force Office of Scientific Research (AFOSR)(FA9550-10-1-0286) and the National Science Foundation (NSF) (ECCS-0756936).

Data Availability Statement

The data that support the findings of this study are available from the corresponding author upon reasonable request.

Disclosures

The authors declare no conflicts of interest.

Notes and references

1 R. M. Wood, *Laser-Induced Damage of Optical Materials*, Taylor & Francis, Boca Raton, 2003.

2 E. W. Taylor, J. E. Nichter, F. D. Nash, F. Haas, A. A. Szep, R. J. Michalak, B. M. Flusche, P. R. Cook, T. A. McEwen, B. F. McKeon, P. M. Payson, G. A. Brost, A. R. Pirich, C. Castaneda, B. Tsap and H. R. Fetterman, *Appl. Phys. Lett.*, 2005, **86**, 201122.

3 D. Avnir, D. Levy and R. Reisfeld, *J. Phys. Chem*, 1984, **88**, 5956–5959.

4 E. T. Knobbe, B. Dunn, P. D. Fuqua and F. Nishida, *Appl. Opt*, 1990, **29**, 2729–2733.

5 I. P. Kaminow, L. W. Stulz, E. A. Chandross and C. A. Pryde, *Appl. Opt*, 1972, **11**, 1563–1567.

6 J. F. Rabek and J.-P. Fouassier, *Lasers in Polymer Science and Technology: Applications, Volume I*, CRC Press, 1989.

7 A. Galvan-Gonzalez, M. Canva, G. I. Stegeman, L. Sukhomlinova, R. J. Twieg, K. P. Chan, T. C. Kowalczyk and H. S. Lackritz, *JOSA B*, 2000, **17**, 1992–2000.

8 A. Galvan-Gonzalez, M. Canva, G. I. Stegeman, R. Twieg, K. P. Chan, T. C. Kowalczyk, X. Q. Zhang, H. S. Lackritz, S. Marder and S. Thayumanavan, *Optics Lett.*, 2000, **25**, 332–334.

9 A. Galvan-Gonzalez, M. Canva, G. I. Stegeman, R. Twieg, T. C. Kowalczyk and H. S. Lackritz, *Optics Lett.*, 1999, **24**, 1741–1743.

10 A. Galvan-Gonzalez, G. I. Stegeman, A. K.-Y. Jen, X. Wu, M. Canva, A. C. Kowalczyk, X. Q. Zhang, H. S. Lackritz, S. Marder, S. Thayumanavan and G. Levina, *JOSA B*, 2001, **18**, 1846–1853.

11 A. Galvan-Gonzalez, K. D. Belfield, G. I. Stegeman, M. Canva, S. R. Marder, K. Staub, G. Levina and R. Tweig, *J. Appl. Phys.*, 2003, **94**, 756.

12 D. Rezzonico, M. Jazbinsek, P. GÃŒnter, C. Bosshard, D. H. Bale, Y. Liao, L. R. Dalton and P. J. Reid, *JOSA B*, 2007, **24**, 2199.

13 Q. Zhang, M. Canva and G. Stegeman, *App. Phys. Lett.*, 1998, **73**, 912.

14 G. D. Peng, Z. Xiong and P. L. Chu, *J. Lightwave Technol.*, 1998, **16**, 2365–2372.

15 B. Howell and M. G. Kuzyk, *J. Opt. Soc. Am. B*, 2002, **19**, 1790.

16 B. Howell and M. G. Kuzyk, *Appl. Phys. Lett.*, 2004, **85**, 1901–1903.

17 N. Embaye, S. K. Ramini and M. G. Kuzyk, *J. Chem. Phys.*, 2008, **129**, 054504.

18 S. K. Ramini and M. G. Kuzyk, *J. Chem Phys.*, 2012, **137**, 054705.

19 S. K. Ramini, B. R. Anderson, S. T. Hung and M. G. Kuzyk, *Polymer Chemistry*, 2013, **4**, 4948.

20 B. R. Anderson, S.-T. Hung and M. G. Kuzyk, *Opt. Com.*, 2014, **318**, 180–185.

21 B. R. Anderson, S. K. Ramini and M. G. Kuzyk, *J. Opt. Soc. Am. B*, 2011, **28**, 528–32.

22 B. R. Anderson, S.-T. Hung and M. G. Kuzyk, *J. Opt. Soc. Am. B*, 2013, **30**, 3193–3201.

23 B. R. Anderson and M. G. Kuzyk, *Optical Materials*, 2014, **36**, 1227–1231.

24 S. K. Ramini, *PhD thesis*, Washington State University, 2012.

25 B. R. Anderson, *PhD thesis*, Washington State University, 2013.

26 B. R. Anderson and M. G. Kuzyk, *Phys. Rev E*, 2014, **89**, 032601.

27 B. R. Anderson, S.-T. Hung and M. G. Kuzyk, *J. Opt. Soc. Am. B*, 2015, **32**, 1043–1049.

28 B. Anderson, S. T. Hung and M. G. Kuzyk, *J. Chem Phys.*, 2016, **145**, year.

29 S.-T. Hung, *PhD thesis*, Washington State University, 2015.

30 B. R. Anderson, R. Gunawidjaja and H. Eilers, *J. Opt.*, 2016, **18**, 015403.

31 N. Stubbs, M. Bridgewater, M. Stubbs, A. Kabir, M. Crescimanno, M. G. Kuzyk and N. J. Dawson, *Optical Materials*, 2018, **76**, 11 – 15.

32 S.-T. Hung, S. K. Ramini, D. G. Wyrick, K. Clays and M. G. Kuzyk, SPIE Optics and Photonics: Organic Photonics + Electronics, San Diego, CA.

33 P. Dhakal and M. G. Kuzyk, *Journal of Photochemistry and Photobiology A*, 2016, **328**, 66–76.

34 S.-T. Hung, A. Bhuyan, K. Schademan, J. Steverlynck, M. D. McCluskey, G. Koeckelberghs, K. Clays and M. G. Kuzyk, *The Journal of Chemical Physics*, 2016, **144**, year.

35 B. R. Anderson, S. K. Ramini and M. G. Kuzyk, SPIE Laser Damage Symposium Proc., Boulder, CO, 2011.

36 P. Kobrin, R. Fisher and A. Gurrola, *Appl. Phys. Lett.*, 2004, **85**, 2385.

37 Y. Zhu, J. Zhou and M. G. Kuzyk, *Opt. Lett.*, 2007, **32**, 958–960.

38 L. DesAutels, M. G. Kuzyk and C. Brewer, *Opt. Express*, 2009, **17**, 18808–18819.

39 B. R. Anderson, R. Gunawidjaja and H. Eilers, *Optics Letters*, 2015, **40**, 577–580.

40 B. R. Anderson, R. Gunawidjaja and H. Eilers, *App. Phys. B*, 2015, **120**, 1–12.

41 B. R. Anderson, R. Gunawidjaja and H. Eilers, Advanced Photonics 2015, 2015, p. NS2A.2.

42 M. G. Kuzyk and S. K. Ramini, Nanophotonics and Macrophotonics for Space Environments VI, 2012.

43 G. L. Fiore, S. J. Rowan and C. Weder, *Chem. Soc. Rev.*, 2013, **42**, 7278–7288.

44 G. O. Wilson, H. M. Andersson, S. R. White, N. R. Sottos, J. S. Moore and P. V. Braun, in *Self-Healing Polymers*, American Cancer Society, 2010.

45 S. Wang and M. W. Urban, *Nature Reviews Materials*, 2020.

46 D. Roy, J. N. Cambre and B. S. Sumerlin, *Progress in Polymer Science*, 2010, **35**, 278 – 301.

47 L. E. Buerkle and S. J. Rowan, *Chem. Soc. Rev.*, 2012, **41**, 6089–6102.

48 C. N. Bowman and C. J. Kloxin, *Angew. Chem. Int. Ed.*, 2012.

49 C. J. Kloxin, T. F. Scott, B. J. Adzima and C. N. Bowman, *Macrmolecules*, 2010, **43**, 2643–2653.

50 R. J. Wojtecki, M. A. Meador and S. J. Rowan, *Nature Materials*, 2011, **10**, 14–27.

51 M. Burnworth, L. Tang, J. R. Kumpfer, A. J. Duncan, F. L. Beyer, G. L. Fiore, S. J. Rowan and C. Weder, *Nature*, 2011, **472**, 334–337.

52 J. D. Fox and S. J. Rowan, *Macromolecules*, 2009, **42**, 6823–6835.

53 I. D. Solovyev, A. V. Gavshina and A. Savitsky, *J. of Biomedical Photonics & Engineering*, 2017, **3**, 040303.

54 J. N. Henderson, H.-w. Ai, R. E. Campbell and S. J. Remington, *Proceedings of the National Academy of Sciences*, 2007, **104**, 6672–6677.

55 D. Sinnecker, P. Voigt, N. Hellwig and M. Schaefer, *Biochemistry*, 2005, **44**, 7085–7094.

56 N. J. Westfall and C. W. Dirk, *Journal of Physical Organic Chemistry*, 2012, **25**, 704–712.

57 B. R. Anderson, S. T. Hung and M. G. Kuzyk, SPIE Optics and Photonics: Optical Engineering + Applications, San Diego, CA, 2012.

58 A. Dubois, M. Canva, A. Brun, F. Chaput and J.-P. Boilot, *App. Optics*, 1996, **35**, 3193–3199.

59 J. F. Rabek, *Polymer Photodegradation: Mechanisms and experimental methods*, Springer-Science+Business Media, 1995.

60 K. Pielichowski and J. Njuguna, *Thermal Degradation of Polymeric Materials*, iSmithers Rapra Publishing, 2005.

61 T. Ichikawa, K. i. Oyama, T. Kondoh and H. Yoshida, *Journal of Polymer Science Part A: Polymer Chemistry*, 1994, **32**, 2487–2492.

62 R. S. Moshrefzadeh, D. K. Misemer, M. D. Radcliffe, C. V. Francis and S. K. Mohapatra, *Appl. phys. lett.*, 1993, **62**, 16–18.

63 S.-C. Chang, G. He, F.-C. Chen, T.-F. Guo and Y. Yang, *App. Phys. Lett.*, 2001, **79**, 2088.

64 P. Annieta, L. Joseph, L. Irimpan, P. Radhakrishnan and V. Nampoori.

65 C. Fellows, U. Tauber, C. Carvalho and C. Carvalhaes, *Brazil-*

ian Journal of Physics, 2005, **35**, 933.
66 A. A. Ishchenko, *Pure Appl. Chem.*, 2008, **80**, 1525–1538.

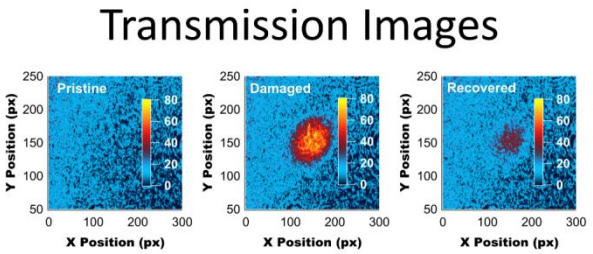

We compare the photodegradation and self-healing characteristics of nine different anthraquinone derivatives doped into PMMA using transmission imaging. Based on the results we determine “rules-of-thumb” to predict enhanced photostability and self-healing for anthraquinones.